

# Synthesis and optical properties of BaTiO<sub>3</sub>:Eu<sup>3+</sup>@SiO<sub>2</sub> glass ceramic nano particles

J. Reyes Miranda · A. García Murillo · F. de J. Carrillo Romo · J. Oliva Uc ·  
C. A. Flores Sandoval · A. de J. Morales Ramírez · S. Velumani ·  
E. de la Rosa Cruz · V. Garibay Febles

Received: 27 January 2014 / Accepted: 22 July 2014  
© Springer Science+Business Media New York 2014

**Abstract** BaTiO<sub>3</sub>:(5 %)Eu<sup>3+</sup> nanoparticles and BaTiO<sub>3</sub>:(5 %)Eu<sup>3+</sup>@SiO<sub>2</sub> composites were synthesized by the solvothermal method. The effects on the structure, morphology and luminescent properties were studied using samples with different molar ratios of BaTiO<sub>3</sub>:(5 %)-Eu<sup>3+</sup>@SiO<sub>2</sub>: 60:40, 50:50, 40:60, 30:70, 20:80, 10:90, 08:92, 6.5:93.5, 05:95, and 1.5:98.5. When the amount of silica in the composites was increased, the orange emission of Eu<sup>3+</sup> increased, too; this was observed by exciting the charge transfer band centered at 283 nm. Furthermore, an increase in the intensity of the emission was obtained under excitation at 394 nm as a consequence of the improvement in the crystallinity of the samples. The presence of silica and the degree of crystallinity of the samples were determined through the Fourier transform infrared spectra and

X-ray diffraction patterns. All of the results suggest that our ceramic material could be a good candidate for biomedical applications such as biolabeling, since the luminescence of BaTiO<sub>3</sub>:(5 %)Eu<sup>3+</sup>@SiO<sub>2</sub> composites have an emission intensity higher than that of nanoparticles composed solely of BaTiO<sub>3</sub>:Eu<sup>3+</sup>. This work demonstrates that BaTiO<sub>3</sub>:Eu<sup>3+</sup>@SiO<sub>2</sub> composites have an emission intensity higher than that of nanoparticles composed solely of BaTiO<sub>3</sub>:Eu<sup>3+</sup>.

**Keywords** Optical materials · Sol–gel chemistry · Electron microscopy · X-ray diffraction · Luminescence

## 1 Introduction

There has been a notable increase in the technological advancement of everyday products that use materials with luminescent properties, from the black-and-white TV of 1936 to the modern TV with LED technology, and from the first lamp made by Edison to the compact fluorescent lamp. It is well known that rare-earth elements such as erbium, terbium, europium, cerium, and ytterbium are the most important activator centers of luminescence, and this has given great impetus to the study of a variety of luminescent materials using a host crystal lattice: oxides, sulfides, selenides, and titanates doped with rare-earth ions. The most important reason for using rare-earth ions as activator centers in matrices is undoubtedly their narrow band of emission and absorption, which is due to  $4f \rightarrow 4f$  electronic transitions [1, 2].

Barium titanate ceramic (BaTiO<sub>3</sub>) has drawn special attention in recent years, due to its excellent dielectric, electro-optic and ferroelectric properties [3]. It is widely used in the microelectronic industry for the fabrication of

---

J. Reyes Miranda · A. García Murillo (✉) · F. J. Carrillo Romo ·  
A. J. Morales Ramírez  
Instituto Politécnico Nacional – CIITEC Azcapotzalco, Cerrada  
de Cecati S/N, Col. Santa Catarina, Del. Azcapotzalco,  
C.P. 02250 Mexico, D.F., Mexico  
e-mail: angarciam@ipn.mx

J. Oliva Uc · E. de la Rosa Cruz  
Centro de Investigaciones en Óptica A.C, León, Gto., Mexico

C. A. Flores Sandoval · V. Garibay Febles  
Programa de Ingeniería Molecular, Instituto Mexicano del  
Petróleo, Eje Central Lázaro Cárdenas 152, Col. San Bartolo  
Atepehuacan, C.P. 07730 Mexico, D.F., Mexico

S. Velumani  
Department of Electrical Engineering (SEES), Centro de  
Investigación y de Estudios Avanzados del IPN, Av. Instituto  
Politécnico Nacional, 2508 Col. San Pedro Zacatenco,  
C.P. 07360 Mexico, D.F., Mexico

capacitors and infrared detectors [4]. In fact, there are reports demonstrating that strong luminescence can be achieved by doping BaTiO<sub>3</sub> with several rare earths, such as Tm<sup>3+</sup>, Yb<sup>3+</sup>, Er<sup>3+</sup> and Eu<sup>3+</sup> [5–7]. Doping BaTiO<sub>3</sub> and other hosts with lanthanides is promising, not only to produce luminescent materials for applications in field emission displays, solid-state lamps and lasers, but also to serve as precursors for grained ceramics, which can be employed in ferroelectric capacitors and thermistors [7–9]. In particular, the Eu<sup>3+</sup> ion has been used as a dopant to illuminate structural changes in BaTiO<sub>3</sub>, as well as to produce luminescent materials in the orange region [8, 10].

Until now, synthesis methods such as solid-state [11], coprecipitation [12], microwave heating [13], the sol–gel, and solvothermal methods have been employed for BaTiO<sub>3</sub> synthesis with a certain degree of crystallinity influencing the final properties [14–16]. Among them, the sol–gel method is widely used because it is a simple method that allows for better control of the size and morphology of the products, and it requires lower temperatures compared to other techniques. Also, the products are obtained are of high purity. However, the precipitates derived from the sol–gel method are usually amorphous, requiring subsequent thermal treatment to induce crystallization. The solvothermal method can yield particles of high purity, high crystallinity and very small size (<30 nm); its chief advantage is its low synthesis temperature, about 200 °C for one-pot synthesis. However, the development of luminescent glass–ceramic composites is an alternative with many advantages. First, there are lower production costs because these composites are mainly derived from silica, which can achieve high homogeneity at low temperatures with the sol–gel method. Second, the combination of ceramics with a silica matrix on a nanometric scale can produce new luminescent properties, which are potentially of practical interest. Although the mechanism that promotes the luminescent properties in glass–ceramic materials has not been extensively studied, it is believed that the interface between the oxide nanoparticles and SiO<sub>2</sub>, in a core/shell configuration, plays a dominant role in emission mechanisms, as well as in defect reduction on the nanoparticle surface [17]. In this context, the solvothermal method was selected as a promising option for preparing the BaTiO<sub>3</sub>:Eu<sup>3+</sup> ceramic powders, while the sol–gel method was chosen to elaborate the SiO<sub>2</sub> shell. To the best of our knowledge, there are no reports on the luminescent and optical properties of BaTiO<sub>3</sub>:Eu<sup>3+</sup> ceramic powders covered with a silica matrix (BaTiO<sub>3</sub>:Eu<sup>3+</sup>@SiO<sub>2</sub>). In this paper, we report the fabrication, morphology, structural and luminescent properties of Eu<sup>3+</sup>-doped BaTiO<sub>3</sub> nanocrystallites embedded in a vitreous matrix for different molar ratios of BaTiO<sub>3</sub>:Eu<sup>3+</sup>@SiO<sub>2</sub>.

## 2 Experimental method

### 2.1 Solvothermal synthesis of BaTiO<sub>3</sub>:Eu<sup>3+</sup> nanoparticles

Most of precursors and solvents employed for the synthesis of BaTiO<sub>3</sub>:Eu<sup>3+</sup> ceramic powders were acquired from Sigma Aldrich and used as received: barium chloride (BaCl<sub>2</sub>, 99.9 %), europium (III) nitrate pentahydrate (Eu(NO<sub>3</sub>)<sub>3</sub>·5H<sub>2</sub>O, 99.9 %), methanol and potassium. Titanium butoxide (Ti[O(CH<sub>2</sub>)<sub>3</sub>CH<sub>3</sub>]<sub>4</sub>, 97 %) was purchased from Fluka. The synthesis procedure for the 5 % europium-doped BaTiO<sub>3</sub> nanoparticles was as follows: First, 1.68 mmol of BaCl<sub>2</sub> was dissolved in anhydrous methanol for 2 h under vigorous magnetic stirring (solution 1). A second solution was prepared by dissolving 0.084 mmol of Eu(NO<sub>3</sub>)<sub>3</sub>·5H<sub>2</sub>O in methanol over 30 min (solution 2). Later, a third solution was made by dissolving 4.10 mmol of K in methanol, with an argon flow, in order to prevent potassium oxidation (solution 3). Afterwards, solution 2 was dropped into solution 1 while stirring, and solution 3 was added after 1 h. Then, titanium butoxide was added drop-wise, using a 1:6 molar ratio of Ba:Ti, as reported by Boulos et al. [18]. The resulting solution was poured into an autoclave and placed for 24 h in an oven at 200 °C. After this, the powders obtained were washed several times with deionized water and a solution of HCl 0.1 M. Finally, the product was dried in an oven at 100 °C for 24 h, yielding a fine powder of europium-doped barium titanate nanoparticles.

### 2.2 Sol–gel synthesis of SiO<sub>2</sub>

The precursors used were tetraethyl orthosilicate (CH<sub>3</sub>H<sub>2</sub>OO<sub>4</sub>Si, 98 %, TEOS), ethanol (CH<sub>3</sub>CH<sub>2</sub>OH, 99.9 % Ferment), hydrochloric acid (HCl 37.1 %, Ferment) and distilled water. In this procedure, a solution of ethanol/TEOS was prepared with a molar ratio of 4:1, according to Klein's diagram [19]. Later, a solution of distilled water and hydrochloric acid was prepared and kept stirring for 1 h. Finally, this last solution was added to the ethanol/TEOS solution and kept stirring for 21 h.

### 2.3 Synthesis of BaTiO<sub>3</sub>:Eu<sup>3+</sup>@SiO<sub>2</sub> nanocomposites

The BaTiO<sub>3</sub>:Eu<sup>3+</sup> powders previously synthesized were weighed and added to the silica solution in such a way that the following molar ratios for BaTiO<sub>3</sub>:Eu<sup>3+</sup>@SiO<sub>2</sub> were obtained: 60:40, 50:50, 40:60, 30:70, 20:80, 10:90, 08:92, 6.5:93.5, 05:95, and 1.5:98.5. Subsequently, the mixture was placed under ultrasonic agitation for 1 h at room temperature. After this, the samples were dried at 100 °C for 24 h, in order to remove the solvents from the glass

solution, and finally they underwent thermal treatment at 200 °C for 24 h.

#### 2.4 Crystalline structure and morphology

The crystalline structure of the powders obtained was analyzed by means of X-ray diffraction with an automated powder diffractometer (D8 Focus Bruker), using Cu-K $\alpha$  radiation. All the data obtained were between  $10^\circ < 2\theta < 80^\circ$  in steps of  $0.02^\circ$  at room temperature. In addition, the morphology and crystalline structure of the prepared samples were determined using high resolution transmission electron microscopy (HRTEM), JEM-2200FS operating between 80 and 200 keV. The microscope was equipped with an ultra-stable Schottky-type field emitter gun. The samples were grounded, suspended in isopropanol at room temperature, and dispersed with ultrasonic agitation; then, an aliquot of the solution was dropped on a 3-mm diameter lacey carbon copper grid. SEM images were obtained using a JEOL DS-500 apparatus.

#### 2.5 Optical characterization

The emission spectra of samples were obtained under ultraviolet (UV) excitation from a 75-W xenon lamp. The fluorescent emissions were analyzed with an Acton Pro 3500i monochromator (Acton Research Corporation) and a R955 Hamamatsu photomultiplier tube for visible emissions. Pellets were made from the powdered samples, and their fluorescence was measured on the fluorometer under the same conditions of alignment. Using the KBr pellet method on a Perkin Elmer 2000 spectrometer, the IR spectra [Fourier transform infrared (FTIR)] of the samples were found to be in the  $400\text{--}4,000\text{ cm}^{-1}$  range. All optical measurements were made at room temperature.

### 3 Results and discussion

#### 3.1 Structure and morphology of $\text{BaTiO}_3:\text{Eu}^{3+}$ nanoparticles and $\text{BaTiO}_3:\text{Eu}^{3+}@\text{SiO}_2$ composites

Figure 1 shows the FTIR spectrum of the  $\text{BaTiO}_3:\text{Eu}^{3+}$  powders obtained by the solvothermal method. The bands in the  $3,000\text{--}3,600\text{ cm}^{-1}$  range correspond to the stretching vibrations of the hydroxyl groups ( $\nu\text{OH}$ ), due to the presence of water in the sample, and the band around  $1,634\text{ cm}^{-1}$  corresponds to the OH deformation vibrations ( $\delta\text{OH}$ ). The band centered at about  $2,905\text{ cm}^{-1}$  is related to C–H stretching vibrations [20]. In addition, there are two bands, located at  $1,450$  and  $851\text{ cm}^{-1}$ , associated with  $\text{CO}_3^{2-}$  stretching vibrations and  $\text{CO}_3^{2-}$  deformation vibrations,

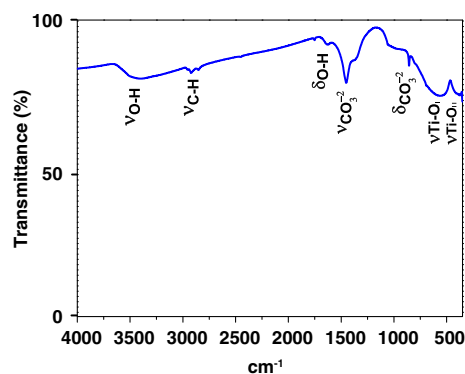


**Fig. 1** FTIR spectra of  $\text{BaTiO}_3:\text{Eu}^{3+}$  powders obtained by solvothermal method

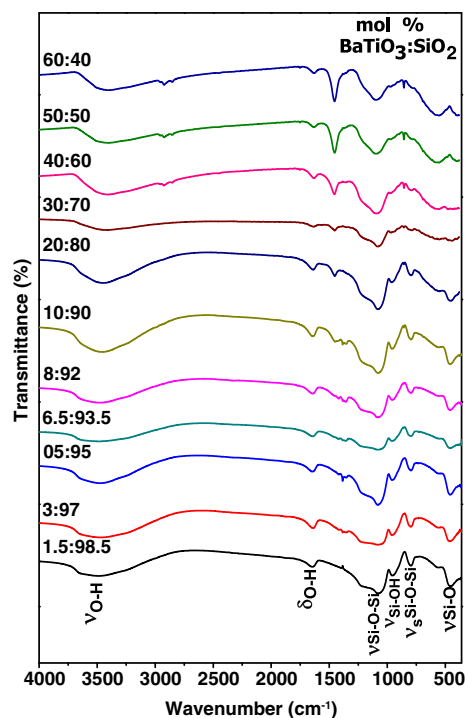


**Fig. 2** FTIR spectra of  $\text{BaTiO}_3:\text{Eu}^{3+}@\text{SiO}_2$  glass ceramic composites

respectively. According to the literature, the latter bands are characteristic of the  $\text{BaCO}_3$  phase [8]. Finally, the bands located at  $577$  and  $383\text{ cm}^{-1}$  are related to the stretching vibrations of  $\nu\text{Ti-O}_1$  and to the torsional vibrations of  $\nu\text{O}_1\text{-Ti-O}_1$  located in the octahedral  $\text{TiO}_6$  of  $\text{BaTiO}_3$  [21].

A change in the bonding of  $\text{BaTiO}_3:\text{Eu}^{3+}@\text{SiO}_2$  composites can be anticipated as a result of the introduction of different molar ratios of silica. Figure 2 shows how the bonding related to the presence of silica disappears as the content of  $\text{BaTiO}_3:\text{Eu}^{3+}$  is increased. The absorption bands centered at  $1,072$  and  $800\text{ cm}^{-1}$  correspond to Si–O–Si

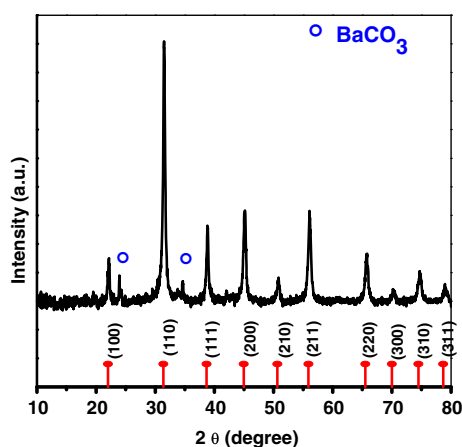


Fig. 3 XRD patterns of  $\text{BaTiO}_3:\text{Eu}^{3+}$  nanoparticles

bonding, and the bands centered at  $954$  and  $450\text{ cm}^{-1}$ , which are associated with Si–OH and Si–O bonding, are predominant for the molar ratios of 20:80, 10:90, 08:92, 6.5:93.5, 05:95, 03:97, and 1.5:98.5; only the band located at  $1,072\text{ cm}^{-1}$  remains in all of the samples. Moreover, when the samples have a molar percentage above 20 % for  $\text{BaTiO}_3$  (samples with molar ratios of 30:70, 40:60, 50:50, 60:40), the bands located at  $577$  and  $383\text{ cm}^{-1}$ , which relate to the stretching vibrations of  $\text{Ti-O}_I$  and to the torsional vibrations of  $\text{O}_I\text{-Ti-O}_{II}$ , respectively, appear again. Furthermore, the peak at  $1,450\text{ cm}^{-1}$  was observed in samples with a composition above 10 molar% for  $\text{BaTiO}_3$ , while the peak at  $851\text{ cm}^{-1}$  appeared for samples with a composition above 20 molar%, whose peaks were associated with the  $\text{BaCO}_3$  phase.

According to the JCPDS card 31-0174, the XRD pattern in Fig. 3 indicates that the Eu-doped  $\text{BaTiO}_3$  perovskite has a cubic phase. This pattern also shows two peaks, at approximately  $24^\circ$  and  $34^\circ$ , which are characteristic of the  $\text{BaCO}_3$  phase. This confirms the presence of that compound, as is suggested by the FTIR spectrum of  $\text{BaTiO}_3:\text{Eu}^{3+}$  in Fig. 1. The crystallite size  $D$  (nm) was estimated using the Scherrer equation [22]; the average size was found to be 23 nm. This is in agreement with the report of Amami et al. [23], who demonstrated that the cubic phase could be obtained only if the particle size is smaller than 30 nm. The XRD patterns of  $\text{BaTiO}_3:\text{Eu}^{3+}@\text{SiO}_2$  glass ceramics in Fig. 4 show the evolution of the peaks corresponding to the cubic phase of  $\text{BaTiO}_3$ , based on the silica content. The composites with molar ratios of 60:40, 50:50, 40:60, 30:70, and 20:80 exhibit high crystallinity, because all of the peaks associated with the cubic phase appear. In fact, those peaks were observed in samples with a molar% above 6.5 % for  $\text{BaTiO}_3$ , while the XRD patterns for samples with a molar% less than 6.5 % for  $\text{BaTiO}_3$ , show only an amorphous phase. Hence, as the concentration of silica

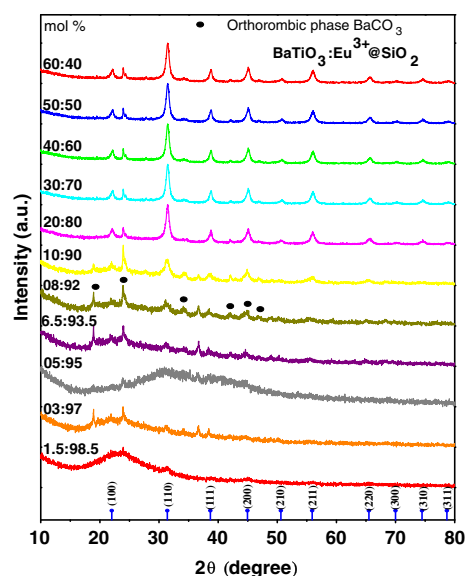


Fig. 4 XRD patterns of  $\text{BaTiO}_3:\text{Eu}^{3+}@\text{SiO}_2$  composites

increases in the glass ceramic, the peaks corresponding to  $\text{BaTiO}_3$  begin to lose intensity and disappear almost completely, because the  $\text{BaTiO}_3$  particles are covered with an amorphous matrix, resulting in a diffractogram that shows poor or no crystallinity.

A SEM image of the 5 % Eu-doped  $\text{BaTiO}_3$  nanoparticles shows spherical particles with an average size of 30 nm (see Fig. 5a). This image also shows agglomerations of  $\text{BaTiO}_3$  nanoparticles, which can be explained by the fact that the particles on the nanometric scale have a high superficial energy; consequently, the probability of coalescence among particles is high [8]. In addition, the stabilization of cubic structures tends to reduce the surface area of growing particles, and this, in turn, can favor the agglomeration of particles. Figure 5b shows a SEM image of the  $\text{BaTiO}_3:\text{Eu}^{3+}@\text{SiO}_2$  glass ceramic with a molar ratio of 5:95; cloudy-like aggregates formed of silica can be seen, about  $1\text{ }\mu\text{m}$  in size, with some large particles of  $\text{BaTiO}_3$  embedded in them. From SEM images corresponding to molar ratios not shown here, it can be concluded that the size of the  $\text{BaTiO}_3:\text{Eu}^{3+}$  nanoparticles embedded in silica increases as the amount of  $\text{SiO}_2$  increases. For example, the sample of  $\text{BaTiO}_3:\text{Eu}^{3+}@\text{SiO}_2$  glass ceramic with a molar ratio of 5:95 was composed of large nanoparticles with an average size of 100 nm, which is about 3.33 times larger than the nanoparticles in the sample without silica (compare Fig. 5a, b).

An HRTEM image of the sample with a molar ratio of 5:95 shows that it is composed of individual crystallites of  $\text{BaTiO}_3:\text{Eu}^{3+}$  with an average size of 10 nm (see Fig. 6a). In fact, the quasi-spherical shape and the nanometric size of the ceramic nanoparticles suggest the presence of the



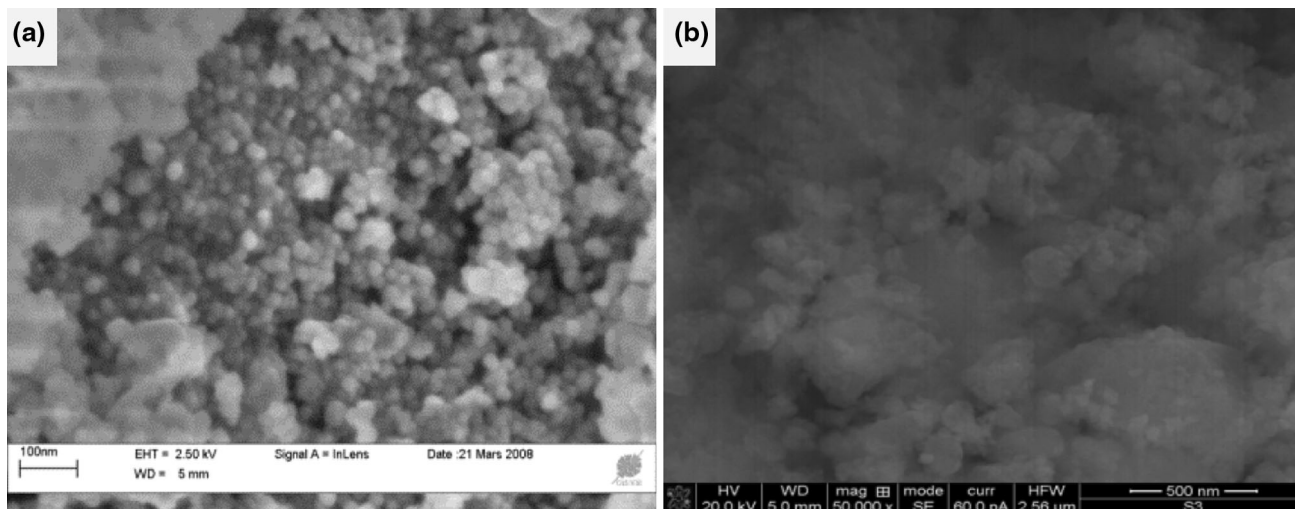


**Fig. 5** SEM images of **a**  $\text{BaTiO}_3:\text{Eu}^{3+}$  nanoparticles and **b**  $\text{BaTiO}_3:\text{Eu}^{3+}@\text{SiO}_2$  composites with a molar ratio of Ba:Si = 5:95

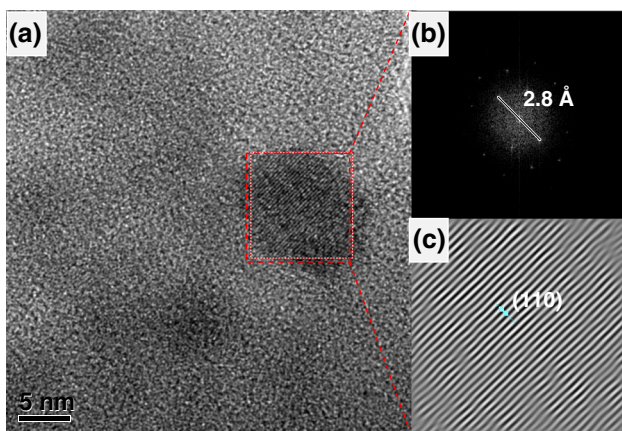


**Fig. 6** **a** HRTEM image for  $\text{BaTiO}_3:\text{Eu}^{3+}@\text{SiO}_2$  composites with a molar ratio of Ba:Si = 5:95. **b** Fast Fourier transform (FFT) of image **(a)** and **c** the crystalline planes corresponding to the direction (110) in  $\text{BaTiO}_3:\text{Eu}^{3+}@\text{SiO}_2$  composites

cubic crystalline phase [24]. The Fourier transform obtained from the image of the nanoparticle observed in Fig. 6a shows the points related to the interatomic planes. From this image, an interplanar distance of 2.8 Å was calculated for the (110) plane, which exhibits a dominant peak in all of the XRD spectra in Fig. 4 (see interplanar distances show in Fig. 6b, c).

### 3.2 Photoluminescence characterization of $\text{BaTiO}_3:\text{Eu}^{3+}$ nanoparticles and $\text{BaTiO}_3:\text{Eu}^{3+}@\text{SiO}_2$ composites

In order to compare the luminescent properties of  $\text{BaTiO}_3:\text{Eu}^{3+}$  nanoparticles with and without silica, the excitation and emission spectra of all samples were obtained. Figure 7

shows the excitation spectra of  $\text{BaTiO}_3:\text{Eu}^{3+}$  nanoparticles and  $\text{BaTiO}_3:\text{Eu}^{3+}@\text{SiO}_2$  composites monitored at 613 nm; two broad bands centered at 283 and 375 nm can be observed, as well as a dominant band centered at 394 nm. The first broad band at 283 nm can be attributed to the charge transfer process between  $\text{Eu}^{3+}$  and  $\text{O}^{2-}$  ions [25]. The second band, centered at 375 nm, could be related to the charge transfer from cationic or anionic defects to  $\text{Eu}^{3+}$  [7, 8], while the band at 394 nm corresponds to  ${}^7F_0 \rightarrow {}^5L_6$  transitions of  $\text{Eu}^{3+}$ . This excitation spectrum also shows that the intensity of the band related to the charge transfer is increasing as the molar% of silica increases. This band can be observed in the range of 90–98.5 molar% for silica, and it is again seen when we have 100 % of  $\text{BaTiO}_3$ . Since the charge transfer band (CTB) is related to  $\text{O}^{2-}$  ions, it can be expected that their intensity would increase as the amount of  $\text{O}^{2-}$  ions increases, which would take place from the silica capping. The XRD measurements in Fig. 4 clearly indicate that there is a majority presence of the amorphous phase in samples with a content of  $\text{SiO}_2$  ranging from 90 to 98.5 molar%. Furthermore, the presence of silica can be corroborated from the FTIR spectra in Fig. 2. Thus, the increments in the intensity of the CTB are due to increments in the content of silica (see the molar ratios of 10:90, 8:92 and 5:95 in Fig. 7). It is also evident that the intensity of the band associated with defects and located at 375 nm decreases with decreases in the silica content. This band can be observed only in the 80–98.5 molar% range for silica; it is not seen in concentrations below 80 %, but the band centered at 394 nm is remarkably enhanced for concentrations above 40 molar% of  $\text{BaTiO}_3:\text{Eu}^{3+}$  (that is, for concentrations of 60 molar% of  $\text{SiO}_2$  and below). Probably, the defects in the composites are formed as the content of  $\text{SiO}_2$  is increased because the Si atoms create bonds with  $\text{O}_2$  atoms located on the surface of

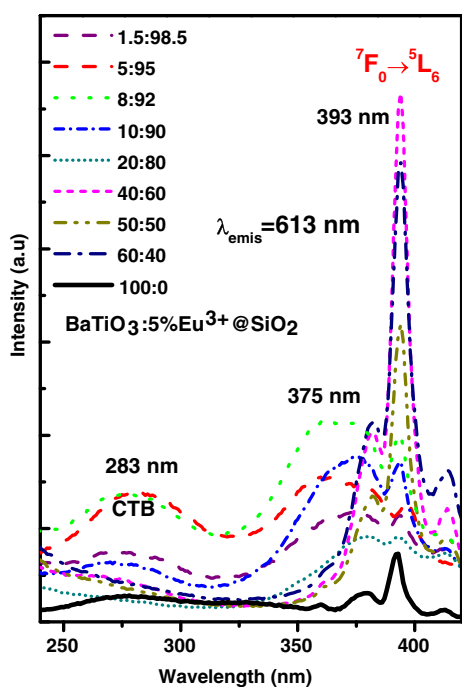


**Fig. 7** Excitation spectra of BaTiO<sub>3</sub>:Eu<sup>3+</sup> nanoparticles and BaTiO<sub>3</sub>:Eu<sup>3+</sup>@SiO<sub>2</sub> composites

the BaTiO<sub>3</sub>:Eu<sup>3+</sup> particles when the crystallites are immersed in the silica solution. Consequently, charge compensation is needed, and anionic or cationic vacancies appear. All these findings suggest that a successive increase of the content of silica in BaTiO<sub>3</sub>:Eu<sup>3+</sup>@SiO<sub>2</sub> composites produces an increase of defects, as well as an enhancement of the charge transfer band. However, below a concentration of 80 molar% of SiO<sub>2</sub> (with the exception of the sample with a 100 molar% concentration of BaTiO<sub>3</sub>:Eu<sup>3+</sup>)—that is, for concentrations of BaTiO<sub>3</sub>:Eu<sup>3+</sup> from 40 molar% and above—the band at 394 nm, corresponding to the <sup>7</sup>F<sub>0</sub> → <sup>5</sup>L<sub>6</sub> transitions, is enhanced. This is caused by an improvement of the crystallinity in BaTiO<sub>3</sub>:Eu<sup>3+</sup>@SiO<sub>2</sub> composites, as indicated by the XRD patterns in Fig. 4 (see the samples with molar ratios of 40:60, 50:50 and 60:40).

The emission spectra in Fig. 8a show the effect of the silica content on the emission of Eu<sup>3+</sup> ions under excitation at 283 nm. The main emission peak at 613 nm can be ascribed to the transition <sup>5</sup>D<sub>0</sub> → <sup>7</sup>F<sub>2</sub>, and the emissions at 577, 592 and 650 nm correspond to the transitions <sup>5</sup>D<sub>0</sub> → <sup>7</sup>F<sub>0</sub>, <sup>5</sup>D<sub>0</sub> → <sup>7</sup>F<sub>1</sub> and <sup>5</sup>D<sub>0</sub> → <sup>7</sup>F<sub>3</sub>, respectively. This figure shows an increase in the emission intensity at 613 nm as the content of silica increases. This trend is evident for samples with a content 80 molar% of silica and above; maximum intensity is reached for the sample with a molar ratio of 5:95, and the emission peak decreases again at a molar ratio of 1.5:98.5. This diminution in intensity could be caused by a deficit of Eu<sup>3+</sup> ions, which might

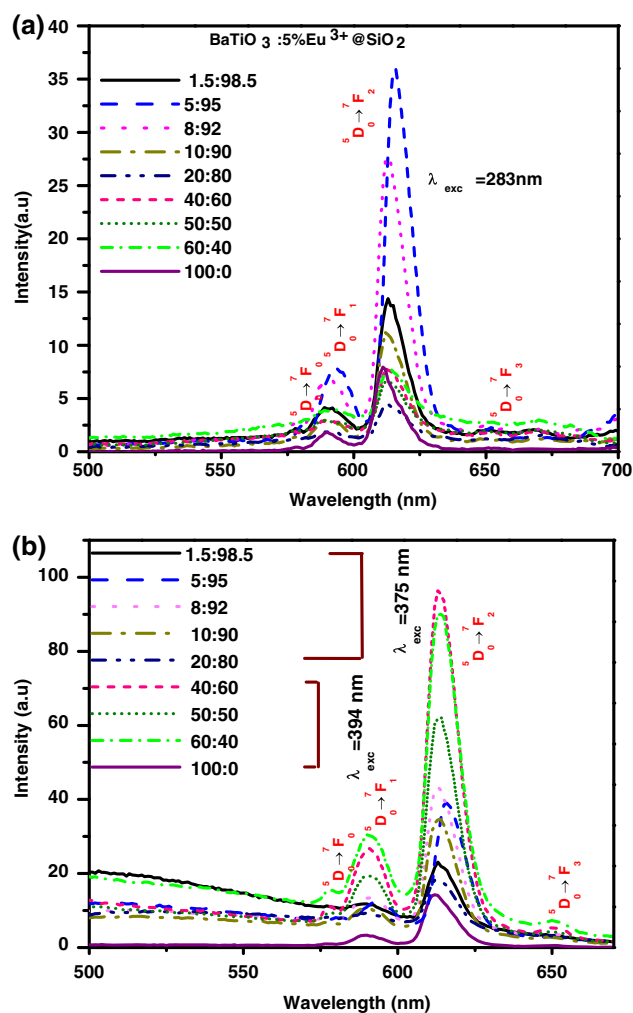


**Fig. 8** Emission spectra of BaTiO<sub>3</sub>:Eu<sup>3+</sup> nanoparticles and BaTiO<sub>3</sub>:Eu<sup>3+</sup>@SiO<sub>2</sub> composites: **a**  $\lambda_{\text{exc}} = 283$  nm and **b**  $\lambda_{\text{exc}} = 394$  nm

receive electrons from O<sup>2-</sup> ions. The small amount of powder used to get a molar amount of 1.5 % for BaTiO<sub>3</sub>:Eu<sup>3+</sup> could produce such a shortage of Eu<sup>3+</sup> ions. It has been reported in studies with Gd<sub>2</sub>O<sub>3</sub>:Eu<sup>3+</sup> nanoparticles coated with silica that the silica is detrimental to emissions, due to a decrease in the refractive index [26, 27]. Therefore, a decrease in luminescence correlating to an increase of SiO<sub>2</sub> could be expected, but this was not observed. In our case, the increase in luminescence could be associated with an increase in the size of the nanoparticles when silica is added. As mentioned above, the size of the nanoparticles increased as the content of silica increased. This was caused by the method used to add silica to the BaTiO<sub>3</sub>:Eu<sup>3+</sup> nanopowders. According to the SEM images, we obtained agglomerations of BaTiO<sub>3</sub>:Eu<sup>3+</sup> nanoparticles covered with silica instead of individual nanoparticles coated with silica, as demonstrated by Liu et al. [26]. An increase in luminescence along with an

increase in size has been observed by Hreniak et al. [28]. Moreover, the increase in luminescence could be provoked by an increase in the amount of  $O^{2-}$  ions, which would be supplied by the gel of silica. As mentioned above, the samples with a molar content of 80 % of silica and above have an enhanced CTB and an additional band related to anionic and cationic defects, which are formed if there is an increase in covalence between the  $O^{2-}$  and the  $Eu^{3+}$ . As a consequence, there is an increase in the energy for electron transfer from  $O^{2-}$  to  $Eu^{3+}$ , which in turn produces an increase in luminescence due to the charge transfer [8, 26]. The CTB of the sample with 100 %  $BaTiO_3:Eu^{3+}$  was also excited, but its emission intensity was lower compared to emissions for samples with a molar content of 90 % silica and above. This clearly indicates that the presence of silica enhances europium emission, due to an improvement in the charge transfer transitions.

Figure 8b shows the emission spectra of the  $BaTiO_3:Eu^{3+}@SiO_2$  composites under excitation at 375 nm for the samples with molar ratios of 1.5:98.5, 05:95, 08:92, 10:90, 20:80, and under excitation at 394 nm for the samples with molar ratios of 40:60, 50:50, 60:40 and 100:0. The excitation spectra show that the bands centered at 283 and 375 nm vanish for samples with a molar percentage of  $BaTiO_3:Eu^{3+}$  at 40 % and above (except for the sample with 100 %  $BaTiO_3:Eu^{3+}$ , which maintains the band at 283 nm); therefore, we decided to excite the samples at 394 nm. This figure also reveals that the emission intensity at 613 nm increases as the molar% of  $BaTiO_3:Eu^{3+}$  increases; these results from the improvement of the cubic crystalline phase, as is apparent in the XRD patterns in Fig. 4 (see the samples with molar ratios of 40:60, 50:50 and 60:40). Furthermore, such an increase in emission can be ascribed to the reduction of the amount of silica compared to the rest of samples (see the FTIR spectra in Fig. 2). Finally, it can be inferred that the emission of  $Eu^{3+}$  produced by excitation of the 394 nm band is more efficient compared to the excitation of the charge transfer band, since the emission intensity of the samples under that excitation is higher than the intensity of those under excitation at 283 nm. For example, compare the emission intensities for samples with molar ratios of 40:60, 50:50, 60:40 in Fig. 8a, b.

#### 4 Conclusion

In this paper, we report a successful procedure for the elaboration of  $BaTiO_3:Eu^{3+}@SiO_2$  composites prepared by the solvothermal and sol-gel methods. The  $BaTiO_3:Eu^{3+}@SiO_2$  composites with Ba:Si molar ratios from 20:80 up to 60:40 showed a cubic phase; conversely, the composites with Ba:Si molar ratios lower than 10:90

revealed an amorphous phase due to the silica shell and some changes in the bonding of the different silica molar ratios, according to the XRD and FTIR results. This work demonstrates that  $BaTiO_3:Eu^{3+}@SiO_2$  composites have an emission intensity higher than that of nanoparticles composed solely of  $BaTiO_3:Eu^{3+}$ . As the molar% of the silica content increases, an enhancement of the charge transfer band occurs, due to the successive introduction of  $O^{2-}$  ions, which are supplied by  $SiO_2$ . Then, when that band is excited, an enhancement in orange luminescence is observed in the samples with the highest content of silica (molar ratios 1.5:98.5, 05:95, 08:92, 10:90 and 20:80), compared to the samples with lower amounts of silica (molar ratios 40:60, 50:50 and 60:40). However, as the amount of silica is decreased and the molar percentage of  $BaTiO_3:Eu^{3+}$  is increased, the CTB tends to disappear, as well as defects in the composites, and the typical emission line of  ${}^5D_0 \rightarrow {}^7F_2$  at  $C_2$  sites of  $Eu^{3+}$  appears. In fact, the crystallinity of composites with no CTB improved, as was confirmed by the XRD measurements for samples with molar ratios of 40:60, 50:50 and 60:40. Such an amelioration of crystallinity gives rise to an increase in luminescence under excitation at 394 nm (compared to the samples with 20 molar% of  $BaTiO_3:Eu^{3+}$  or less). Finally, the results presented in this paper indicate that our material could be a good candidate for biolabeling, since the silica matrix makes the  $BaTiO_3:Eu^{3+}$  nanoparticles biocompatible, and the presence of  $SiO_2$  is not detrimental to the luminescence of the  $BaTiO_3:Eu^{3+}$  nanoparticles.

**Acknowledgments** This work was supported by the IPN through projects SIP-20140031, SIP-20140032. J. Reyes Miranda acknowledges the Ph. D. scholarship from CONACYT. The authors thank the experimental support of CNMN-IPN for structural studies. The authors thank PhD Hageo Desirena Enriquez for his technical support in luminescence studies. The authors also would like to thank Henry Jankiewicz for the editing work that he did for this paper. The authors would also like to thank M. García Murillo for her assistance.

#### References

1. García Solé J, Bausá LE, Jaque D (2005) An introduction to the optical spectroscopy of inorganic solids. Wiley, USA
2. Wybourne BG, Smentek L (2007) Optical spectroscopy of lanthanides. CRC Press, Boca Raton
3. Hu Z, Wang G, Huang Z, Meng X, Chu J (2003) Investigations on the infrared optical properties of  $BaTiO_3$  ferroelectric thin films by spectroscopic ellipsometry. *Semicond Sci Technol* 18:449–453
4. Mahata MK, Kumar K, Rai VK (2014) Structural and optical properties of  $Er^{3+}/Yb^{3+}$  doped barium titanate phosphor prepared by co-precipitation method. *Spectrochim Acta, Part A* 124: 285–291
5. Liu Y, Pisarski WA, Zeng S, Xu C, Yang Q (2009) Tri-color upconversion luminescence of rare earth doped  $BaTiO_3$  nanocrystals and lowered color separation. *Opt Express* 17(11): 9089–9098

6. Li J, Kuwabara M (2003) Preparation and luminescent properties of Eu-doped BaTiO<sub>3</sub> thin films by sol-gel process. *Sci Tech Adv Mater* 4:143–148
7. Rabuffetti FA, Culver SP, Lee JS, Brutchey RL (2014) Local structural investigation of Eu<sup>3+</sup>-doped BaTiO<sub>3</sub> nanocrystals. *Nanoscale* 6:2909–2914
8. Patel DK, Vishwanadh B, Sudarsan V, Vatsa RK, Kulshreshtha SK (2011) Hexagonal BaTiO<sub>3</sub>:Eu<sup>3+</sup> nanoparticles: a kinetically stable phase prepared at low temperatures. *J Am Ceram Soc* 94(2):482–487
9. Rodriguez-Garcia CE, Perea-Lopez N, Hirata GA, DenBaars SP (2008) Red-emitting SrIn<sub>2</sub>O<sub>4</sub>:Eu<sup>3+</sup> phosphor powders for applications in solid state white lamps. *J Phys D* 41:092005
10. Jadhav AP, Pawar AU, Palc U, Kang YS (2014) Red emitting Y<sub>2</sub>O<sub>3</sub>:Eu<sup>3+</sup> nanophosphors with > 80% down conversion efficiency. *J Mater Chem C* 2:496–500
11. Busca G, Buscaglia V, Leoni M, Nannit P (1994) Solid-state and surface spectroscopic characterization of BaTiO<sub>3</sub> fine powders. *Chem Mater* 6(7):955–961
12. Duran P, Capel F, Gutierrez D, Tartaj J, Banares MA, Moure C (2001) Metal citrate polymerized complex thermal decomposition leading to the synthesis of BaTiO<sub>3</sub>: effects of the precursor structure on the BaTiO<sub>3</sub> mechanism. *J Mater Chem* 11(7):1828–1836
13. Ma Y, Vileno E, Suib SL, Dutta PK (1997) Synthesis of Tetragonal BaTiO<sub>3</sub> by Microwave heating and conventional heating. *Chem Mater* 9(12):3023–3031
14. Zhu X, Zhu J, Zhou S, Liu Z, Ming N, Dietrich H (2005) BaTiO<sub>3</sub> nanocrystals: hydrothermal synthesis and structural characterization. *J Cryst Growth* 283(3–4):553–562
15. Wada S, Nozawa A, Ohno M, Kakemoto H, Tsurumi T, Kameshima Y, Ohba Y (2009) Preparation of barium titanate nanocube particles by solvothermal method and their characterization. *J Mater Sci* 44(19):5161–5166
16. García-Hernández M, Chadeyron G, Boyer D, García-Murillo A, Carrillo-Romo F, Mahiou R (2013) Hydrothermal synthesis and characterization of europium-doped barium titanate nanocrystallites. *Nano-Micro Lett* 5(1):57–65
17. Pang T, Cao W, Xing M, Feng W, Xu S, Luo X (2011) Preparation and upconversion luminescence of monodisperse Y<sub>2</sub>O<sub>3</sub>:Yb/Ho-silica/aminosilane core-shell nanoparticles. *J Rare Earth* 28(4):509–512
18. Boulos M, Guillermet-Fristch S, Matheieu F, Durant B, Lebey T, Bley V (2005) Hydrothermal synthesis of nanosized BaTiO<sub>3</sub> powders and dielectric properties of corresponding ceramics. *Solid State Ion* 176(13–14):1301–1309
19. Klein LC (1985) Sol-gel processing of silicates. *Annu Rev Mater Sci* 15:227–248
20. Du H, Wohlrab S, Weib M, Kaskel S (2007) Preparation of BaTiO<sub>3</sub> nanocrystals using a two-phase solvothermal method. *J Mater Chem* 17:4605–4610
21. Last JT (1957) Infrared-absorption studies on barium titanate and related materials. *Phys Rev* 105(6):1740–1750
22. Cullity BD (1978) *Elements of X-ray diffraction*. Addison-Wesley, Reading
23. Amami J, Hreniak D, Guyot Y, Pazik R, Streck W, Goutaudier C, Boulon G (2007) New optical tools used for characterization of phase transitions in nonlinear nano-crystals. Example of Yb<sup>3+</sup>-doped BaTiO<sub>3</sub>. *J Phys Condens Matter* 19(9):1–14
24. Matsui K, Noguchi T, Islam NM, Hakuta Y, Hayashi H (2008) Rapid synthesis of BaTiO<sub>3</sub> nanoparticles in supercritical water by continuous hydrothermal flow reaction system. *J Cryst Growth* 310(10):2584–2589
25. Dutta DP, Ballal A, Nuwad J, Tyagi AK (2014) Optical properties of sonochemically synthesized rare earth ions doped BaTiO<sub>3</sub> nanophosphors: probable candidate for white light emission. *J Lumin* 148:230–237
26. Liu T, Wanga Y, Qin H, Bai X, Dong B, Sun L, Song H (2011) Gd<sub>2</sub>O<sub>3</sub>:Eu<sup>3+</sup>@mesoporous SiO<sub>2</sub> bifunctional core-shell composites: fluorescence label and drug release. *Mater Res Bull* 46:2296–2303
27. Liu G, Hong G, Sun D (2004) Synthesis and characterization of SiO<sub>2</sub>/Gd<sub>2</sub>O<sub>3</sub>:Eu core-shell luminescent materials. *J Colloid Interface Sci* 278:133–138
28. Hreniak D, Streck W, Amami J, Guyot Y, Boulon G, Goutaudier C, Pazik R (2004) The size-effect on luminescence properties of BaTiO<sub>3</sub>:Eu<sup>3+</sup> nanocrystallites prepared by the sol-gel method. *J Alloys Compd* 380:348–351